Modeling of Resistance Spot Weld Nugget Growth

Finite element model takes into account mechanical behavior as well as transient thermal responses of RSW

BY C. L. TSAI, O. A. JAMMAL, J. C. PAPRITAN AND D. W. DICKINSON

ABSTRACT. The weld nugget in resistance spot welding of Type 347 stainless steel was found, using finite element methods, to initiate in a ring shape at a distance from the electrode center. The ring-like weld nugget expands inward and outward during the welding cycles. The welding current, electrode pressure and hold time affected the thermomechanical interactions of the welding process and changed the final nugget geometry. Also, when spot welding workpieces of unequal thicknesses, it was found that the weld nugget formed mostly in the thicker workpiece than in the thinner workpiece, and when spot welding dissimilar materials, the weld nugget formed more in the workpiece of lower thermal conductivity or higher electrical resistivity.

Introduction

The resistance spot welding process has been widely used in the mass production industries, where long production runs and consistent conditions can be maintained. The automotive industry is the major user of this welding process, followed by the appliance industry. It is also used by many industries manufacturing a variety of products made of thin gauge metals (Refs. 1–4).

To improve the productivity of resistance spot welded parts, process automation with sensors and feedback controls is of great interest to end users. Sensors are used to monitor welding current, electrode pressure and hold time, as well as the nugget growth during the welding process. Microcomputers are used to analyze the data, compare them with the programmed operational tolerances and send instructions to the controller to adjust the welding parameters in-process accordingly.

Recently, many studies on resistance spot welding have been reported (Refs. 5–10). These studies were either experimental or numerical, but with the same objective to develop an automation system with a control algorithm.

The thermomechanical coupling of the resistance spot welding process is a complicated phenomena that involves mechanical, electrical, thermal and metallurgical factors. These factors, individually or combined, have a major influence on the state of stress attained during the squeeze, weld and hold cycles, as well as on weld nugget formation and final nugget geometry. In order to develop the appropriate automation mechanisms, understanding these complicated phenomena and analyzing the major factors and parameters involved in the resistance spot welding process are necessary.

A mathematical model can be utilized to analyze the resistance spot welding process and make use of the computational power of today's computers to employ complex mathematical formulations to simulate the welding process according to physical laws. Once verified, it can be used to explain the observed experimental phenomena, to provide insights into the local material response for selecting process parameters, and to minimize the amount of experimental work.

In this paper, the resistance spot welding process was modeled and simulated using the finite element code ANSYS. The mechanical behavior of the process coupled with the transient thermal responses during spot welding was analyzed. The weld nugget formation in resistance spot welding of Type 347 stainless steel of equal and unequal thicknesses, and of Type 347 stainless steel to AISI 1045 carbon steel was studied.

C. L. TSAI and D. W. DICKINSON are with the Department of Welding Engineering and J. C. PAPRITAN is with the Department of Agricultural Engineering, Ohio State University, Columbus, Ohio. O. A. JAMMAL is with Automated Analysis Corp., Peoria, Ill.

Paper presented at the 71st AWS Annual Meeting, held April 22–27, 1990, in Anaheim, Calif.

KEY WORDS

Modeling
RSW Nugget Growth
Resistance Spot Weld
Finite Element Model
Thermomechanical Factors
Stainless Steel
Stress Distribution
Weld Cycle
Welding Parameters
ANSYS Code

Literature Review on Process Simulations

The simulation of the resistance spot welding process through analytical models has drawn the attention of many researchers. Early mathematical modeling however, was unable to achieve comprehensive analysis of the process due to its complexity, which involves the interaction of mechanical, electrical, thermal, metallurgical and surface phenomena. Most of the attempts made to simulate the process via mathematical and theoretical models were mainly directed to heat transfer problems and surface phenomena while neglecting the thermomechanical responses.

The behavior of contact resistance due to electric current flow in conducting solids was studied theoretically by Bowden and Williamson (Ref. 11) in 1958. Their study revealed that surface aspirates produce constricting resistance at the contact between two solid surfaces, and the temperature rise at the interface due to current flow will soften the metal locally and eventually increase the contact area.

Greenwood and Williamson (Ref. 12) elaborated on the subject and conducted an experimental and theoretical investigation to determine current distribution over a small area between two semi-infinite solids in contact. They reported current density singularities at the outer rim of the contact area from theory and correlated this phenomenon with experimental results, which showed heat concentration at the periphery. They concluded that the bulk of the material near the contact region is not heated appreciably by the flow of current through it. It is heated indirectly by conduction from the peripheral region of the contact area.

One step further was taken by Archer (Ref. 13) in 1960. Archer mathematically studied the temperature response in spot welds from a process control viewpoint. He made several assumptions, which oversimplified the problem, but provided insights into the dynamic response of the material to heating conductions.

In 1961, Greenwood (Ref. 14) introduced the first heat conduction model using the finite difference method to simulate the resistance spot welding process. This work is considered a vital contribution to the analytical modeling of the process. Greenwood developed an asymmetric heat conduction model and included internal Joule heating, although his model did not account for heat generation due to contact resistance and ignored the latent heat of fusion during phase transformation. He did consider temperature-independent material properties. The results showed spatial temperature distributions over the time range of the welding cycles. These results indicated that a temperature concentration at the periphery of the electrode/workpiece interface occurs early in the weld cycle. At longer times, the temperature distribution along the workpiece/workpiece interface resembled the shape of an elliptical nugget.

Later, Bentley and Greenwood (Ref. 15) studied theoretically and experimentally the effect of contact resistance on the temperature distribution at different times in the weld cycle during the formation of spot welds in mild steel specimens. The mathematical model previously developed by Greenwood (Ref. 14) was used to compare the predicted temperature distributions with the actual experimental results. The conclusion drawn by the study indicated that the contact resistance played a major role only in the early stages of heat production and became less influential in the later stages of the weld nugget formation. Greenwood's model, however, did not include the contact resistance, thereby ignoring the experimental results in the early stages of the welding cycles, but it did provide good indications of actual temperature patterns at the later stages.

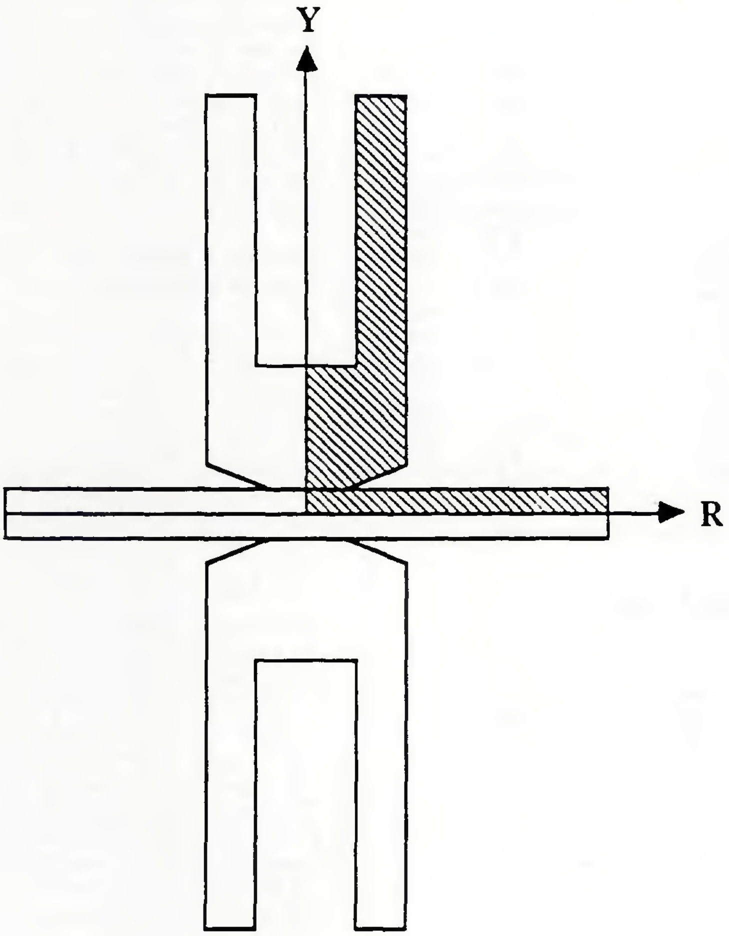

Fig. 1— Geometry of axisymmetric model.

In 1967, Rice and Funk (Ref. 16) analytically investigated the temperature distributions during resistance spot welding of composite materials and related the effect of contact resistance to the temperature distribution throughout the welding cycle. They formulated a one-dimensional multilayer heat transfer model and used the difference equations method of analysis. The model accounted for temperature-dependent material properties, energy generation due to bulk Joule heating, and contact resistance at the interfaces. However, their model did not include the latent heat of fusion for melting. Their results showed that contact resistance is of very little influence during the early stages of the weld cycle. They concluded, though, that during the bulk of the welding time the contact resistance is almost near the final value.

Two analytical models using the finite difference numerical technique was developed by Houchens, *et al.* (Ref. 5), in 1977. Their models simulated the resistance spot welding process to investigate the thermal response and weld nugget penetration during the spot welding of steel sheets. The first was a one-dimensional heat transfer model, which accounted for temperature-dependent material properties, latent heat of fusion and Joule heating for both electrode and workpiece. The second was an asymmetric model, which included the geometric effects of a flat end electrode. The results from the two models indicated that the first model provided insights into factors that influence weld formation and nugget growth, while the second model provided information on current density and temperature distributions.

Gould (Ref. 6) investigated weld nugget development during spot welding three different gauges of AISI 1008 steel using both experimental examination and analytical techniques. He used a one-dimensional heat transfer model similar to the one used by the previous authors (Refs. 4, 5). His model took into consideration the following: electrode geometry, temperature-dependent material properties, melting, internal heat generation and contact resistance. A finite difference technique was employed to obtain solutions for the nonlinear differential equations. Comparison between the analytical results and the metallographic examination of the heavy gauge specimens showed a discrepancy in the model, which predicted nugget sizes much larger than those observed in the experiment. The discrepancy reported was related to the model's inherent inability to account for axial heat flow into the sheet.

In the aforementioned publications, it is evident the thermomechanical coupling of the resistance spot welding process was totally ignored. All the mathematical models reported by the cited authors have been devoted to analyzing the thermal behavior of the process under different sets of parameters while neglecting the major role of the mechanical and thermal stresses involved in the process.

In 1984, Nied (Ref. 7) used ANSYS and introduced an asymmetric model, which included the geometry of the electrode and workpiece and accounted for temperature-dependent thermal properties, melting and Joule heating. Predictions of electrode and workpiece deformations were illustrated and stress distributions along the interfaces were also obtained. The thermal analysis provided temperature distributions showing the characteristic isotherms of an elliptic-shaped weld nugget. Although the model accounted for both mechanical and thermal responses of the welding process, the simulation of contact resistance and the thermomechanical coupling were not clearly explained.

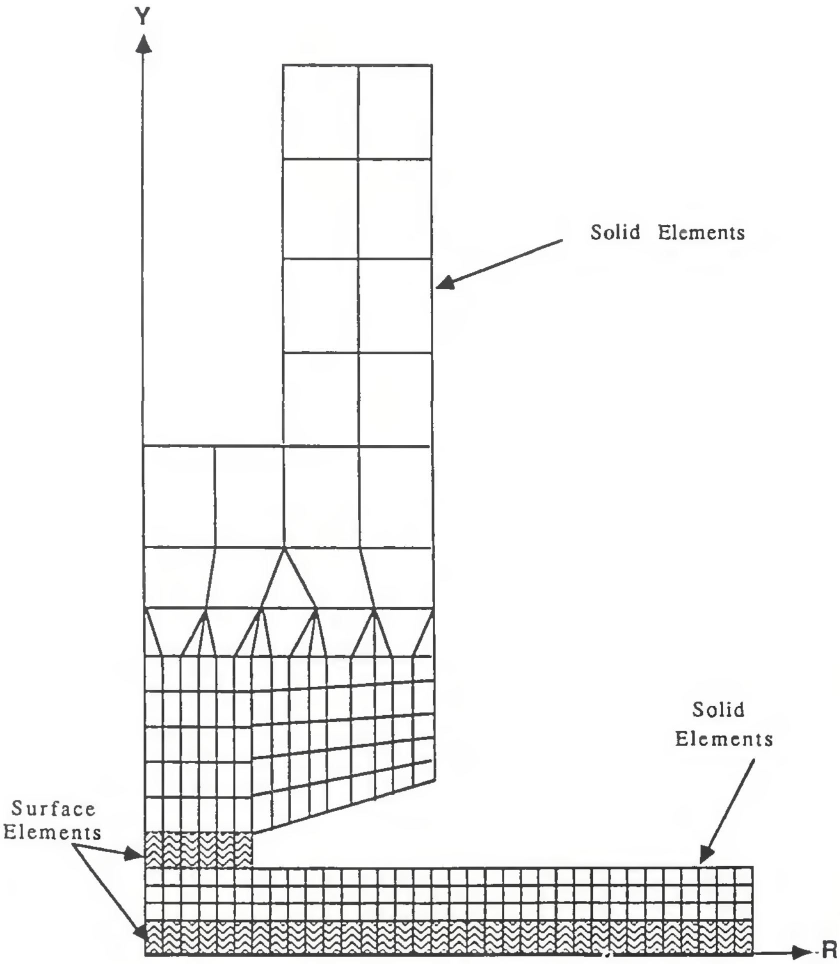

Fig. 2 — Finite element model identifying element types.

Finite Element Model for Current Study

Geometric Modeling

Considering a typical arrangement for spot welding two pieces of sheet metal, the development of a geometric representation of two identical electrodes and equal thickness workpieces simplifies the geometry to a two-dimensional asymmetric model. Only one quadrant of the model, the shaded area in Fig. 1, has to be constructed.

Figure 2 shows the two-dimensional finite element mesh structure used for the analysis. The three element types were: thermoelectric solid element for thermal analysis, isoparametric solid element for stress analysis, and surface element for coupling.

The thermoelectric solid element was used to account for the resistance heating in the workpieces and to calculate the temperature history and distribution during the weld cycles. The calculated temperatures were imposed on the isoparametric solid elements through computer coupling routines and calculations continued for stresses developed from thermal strains and electrode squeezing. The surface element, with its thickness considered equal to a typical oxide thickness, about 0.002 in. (0.05 mm), was used to simulate the coupling effects of the thermomechanical phenomena between electrode/workpiece and workpiece/workpiece.

The mesh structure consists of 334 nodes and 285 elements. The element mesh size at the end of the electrode and for the workpiece is sufficiently refined to account for steeper stress and thermal gradients in that region. A coarser mesh is considered in the upper region of the electrode where the gradients are shallower because of heat conduction to the water-cooling channel.

Boundary Conditions

The purpose of imposing boundary conditions on the model was to stimulate the physical interactions experienced by the material and its surroundings. Two sets of assumptions were made in the model and specified as boundary conditions, one pertaining to the stress analysis and the other regarding the thermal analysis. The boundary conditions are summarized below.

Thermal Analysis

1) The electrical boundary conditions assumed voltage drop between the top end of the electrode and the interface of the workpieces.

2) Current flow was permitted across the contact area of electrode and workpiece, while no current flow was permitted along the lateral surfaces and centerline of the electrode.

3) Convective heat transfer to ambient temperature was specified on all lateral surfaces of electrode and workpiece except at the contact area and along the centerline.

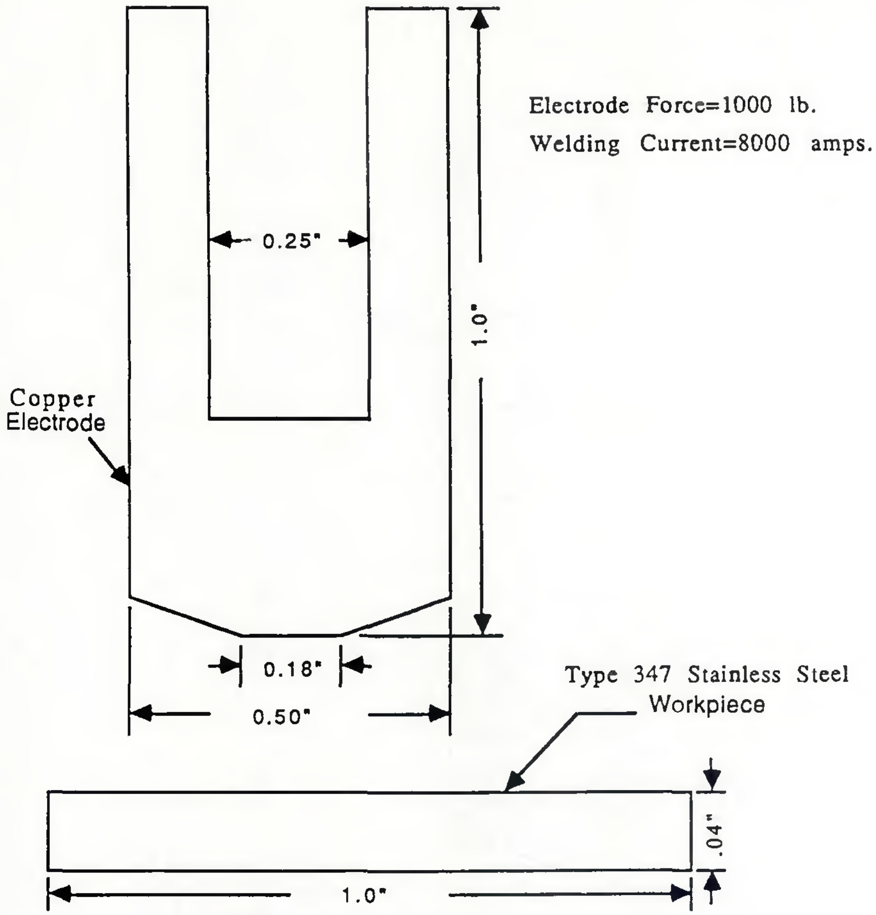

Fig. 3 — Configuration and dimensions of electrode and workpiece.

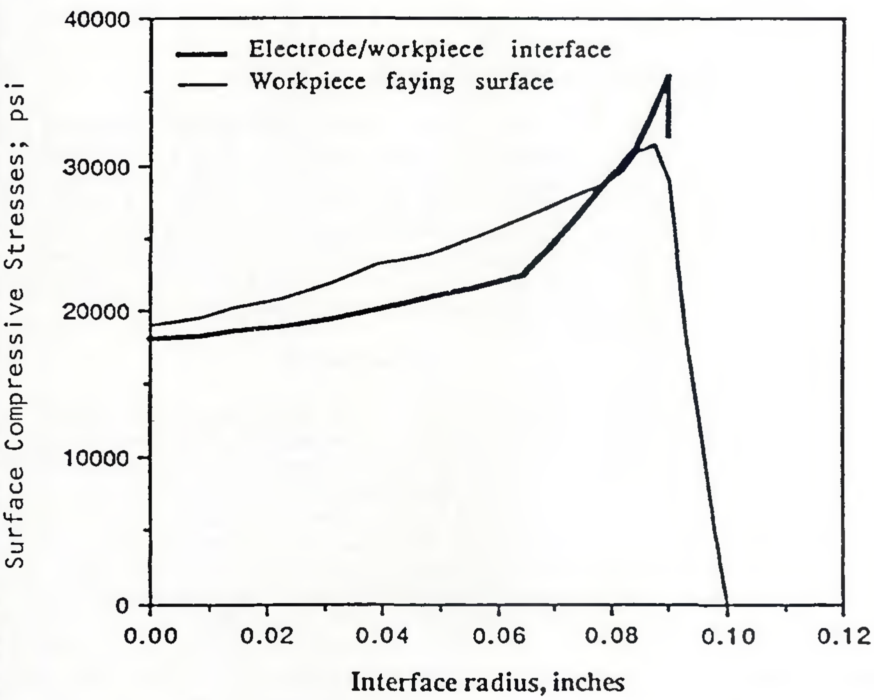

Fig. 4 — Stress distribution along electrode/workpiece interface and workpiece faying surface. (applied load: 1000 lb)

4) Convective heat transfer to the water-cooling channel was specified in the cavity of the electrode.

5) There was no heat flow along the centerline or along the contact area of the workpieces because of asymmetry.

Structural Analysis

1) The application of electrode load assumed a pressure distribution across the annular end of the electrode.

2) Normal displacement at the contact area of the workpieces was restricted because of asymmetry.

3) Radial displacement was restricted along the centerline.

Process Simulation

A truncated copper electrode (Class III) and sheets of 347 stainless steel were chosen for the analytic experiment. Figure 3 shows the dimensions and configurations of both electrode and workpiece. The results obtained from the analytical model were compared with the existing data and schedules for spot welding sheets of stainless steel (Ref. 2).

Squeeze Cycle

The electrode and workpiece deformation after the application of a contact load of 1000 lb (454.5 kg) was calculated. The penetration of the electrode into the workpiece represents the extent of indentation, which occurred over an area of 4.1 X 10^{-5} in. radius. The electrode load produced local stain, which caused the outer edges of the workpiece to separate. This result confirms early analytical results obtained by Civelek (Ref. 17) and Ned (Ref. 7).

The stress distributions obtained along the electrode/workpiece interface and the workpiece faying surface are shown in Fig. 4. A maximum normal stress of 36 ksi (248 kPa) is depicted at the outer rim of the interface. Along the workpiece faying surface however, a maximum normal stress of 31.5 ksi (217 kPa) is also noticed at the periphery of the contact region. These results indicate that the stresses are not uniformly distributed; they start at a lower value at the center and increase in the radial direction. This variation in stress distribution is attributed to the assumption of a nonrigid electrode material; otherwise, stress singularities would have occurred in the workpiece at the edge of the electrode. This phenomenon has also been observed by Nied (Ref. 7).

These high stresses at the periphery of contact have a pinching effect, which prevents molten metal expulsion. However, under repetitive loading, electrode deterioration and mushrooming would

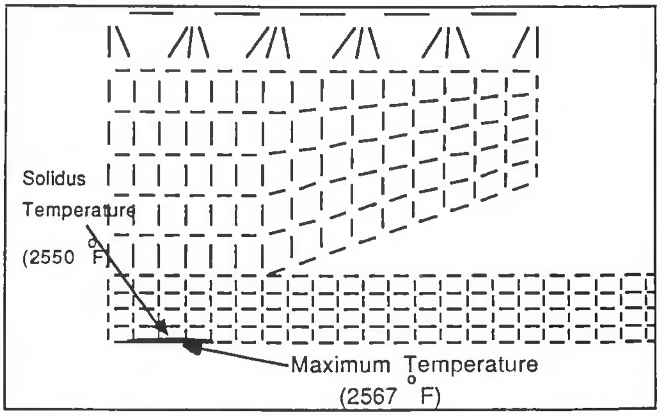

Fig. 5 — Initial nugget formation offset from center. (2.75 cycles, 8000 A)

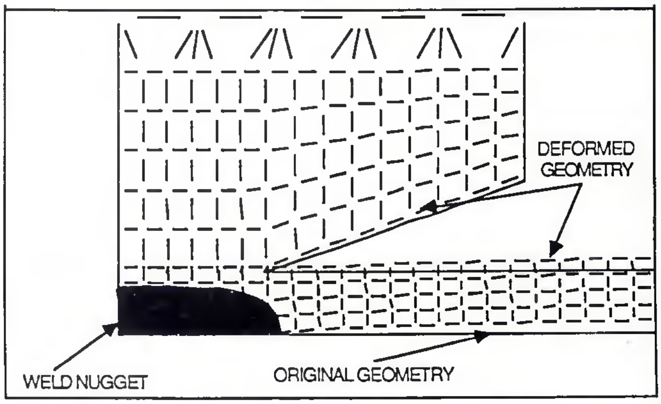

Fig. 6 — A well developed weld nugget. (6 cycles, 8000 A)

be expected. Therefore, the maximum electrode load needs to be limited to prevent premature electrode failure.

Under these compressive stresses, the contact diameter between the electrode and workpiece is found to be 0.18 in. (4.6 mm), which is essentially equal to the electrode face diameter. However, the contact diameter between the workpieces is found to be 0.20 in. (5.1 mm). It is obvious from these results that assuming a contact diameter at the interface of workpieces equal to the electrode face diameter is a possible source of error.

Weld Cycle

A voltage drop equal to 0.5 V between the upper electrode and the interface of the workpieces was assumed at the beginning of the welding cycle. The total voltage drop across the two electrodes was experimentally determined to be 1.0 V based on an applied current of 8000 A from a single-phase power source at 60 Hz. The reference ambient temperature of air was set equal to 70°F (21°C) and the temperature of the cooling water in the electrode cavity was specified as 50°F (10°C). The surface convection coefficient between the lateral surfaces and the air was specified equal to 9E-6 Btu/s in.^{2} °F. During the welding cycle, the applied load was maintained constant, and the weld nugget development was monitored by plotting the nugget isotherms at different weld cycles. Figures 5 and 6 show the weld nugget at 2.75 cycles and 6 cycles, respectively. Figures 7 and 8 show the temperature distribution, at 2.75 cycles, along workpiece faying surface and electrode/workpiece interface, respectively.

Figure 5 shows that the weld nugget essentially forms as a toroid about the centerline. In a very short time (0.003 s) after initial melting has occurred at 2.9 cycles, the molten region spread rapidly toward the center and formed an elliptic-shaped nugget with only a little noticeable outward growth.

At the end of 6 cycles, the nugget growth is equal to 0.195 in. (4.9 mm) in nugget diameter with 67.5% penetration — Fig. 6. This nugget size falls within the range recommended by the Resistance Welder Manufacturers' Association (RWMA) (Ref. 1). This nugget size is produced at the same number of weld cycles suggested by the RWMA. The general behavior of weld nugget growth compared with existing experimental data is shown in Fig. 9. The nugget diameter is plotted against weld cycles. The data points were obtained from various weld cycles producing a weak nugget up to expulsion. The finite element model has predicted the behavior of weld nugget growth in a very similar manner.

As shown in Fig. 7, after 2.75 cycles, the temperature is maximum at a position away from the centerline along the workpiece faying surface. The maximum temperature is in the liquidous range of stainless steel. Along the electrode/

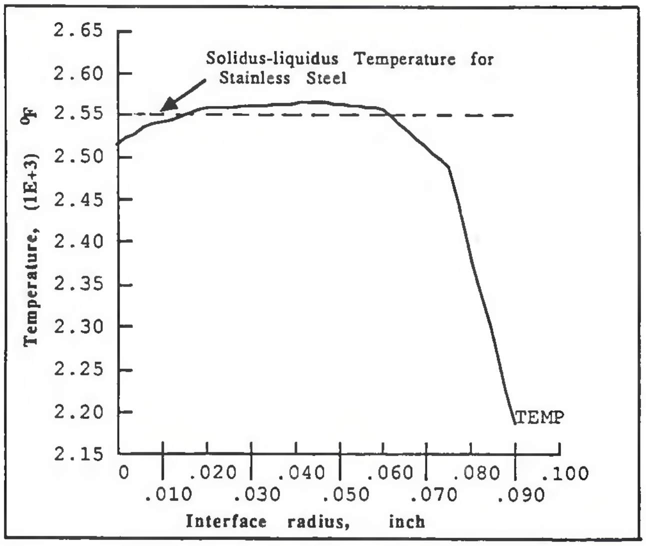

Fig. 7 — Temperature distribution along workpiece faying surface after 2.75 cycles. (8000 A)

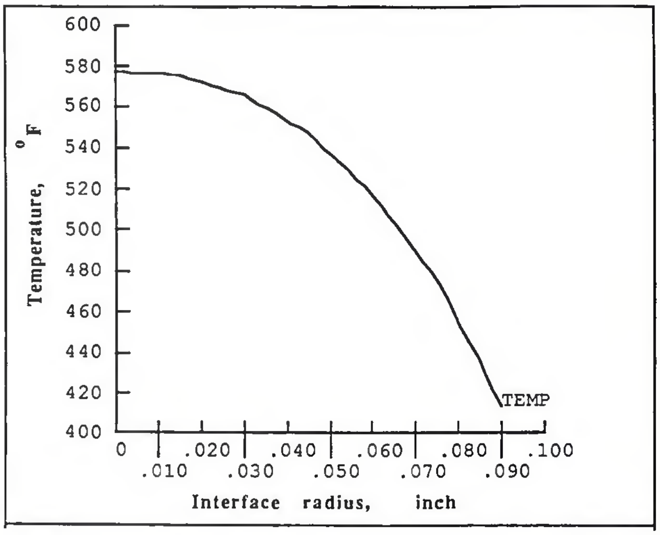

Fig. 8 — Temperature distribution along electrode/workpiece interface after 2.75 cycles. (8000 A)

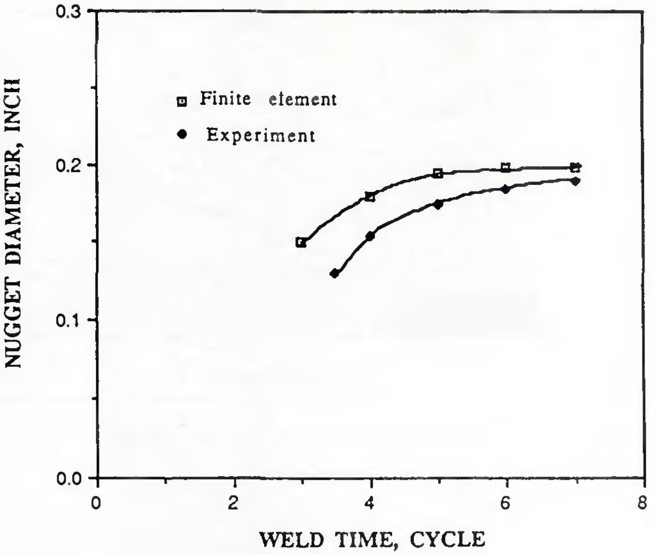

Fig. 9 — Weld nugget diameter as a function of weld time.

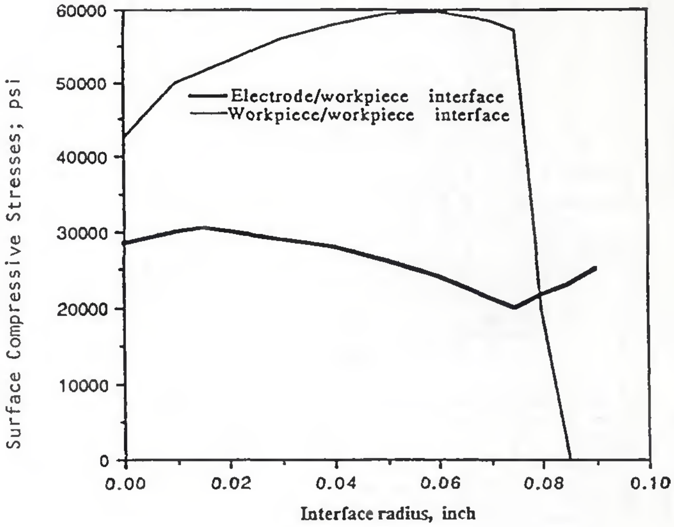

Fig. 10 — Stress distribution along electrode/workpiece interface and workpiece faying surface at the end of ten hold cycles. (8000 A)

workpiece interface (Fig. 8), the maximum temperature is at the center and drops to lower values at the periphery.

Hold Cycle

Thermal stresses and stresses from the loading pressure cause stress distributions along the electrode/workpiece interface and workpiece faying surface. Fig. 10 shows these stress distributions at the end of 10 hold cycles.

The maximum compressive stress obtained along the electrode/workpiece interface is near the center and equal to 30 ksi (206.8 kPa). Close to the edge of this interface, the compressive stress drops down to a minimum value of 20 ksi (137.9 kPa). Comparing these results with the results obtained during the squeeze cycle indicate that the drop in compressive stress at the periphery of the electrode/ workpiece interface is attributed to the plastic deformation induced by the thermal stresses developed during the welding cycle coupled with the mechanical stress applied by the electrode load. The increase in compressive stress toward the center, however, is due to weld nugget thermal expansion. The stress at that region was increased from about 17.5 ksi (120.6 kPa) during the squeeze cycle up to 30 ksi at the end of the hold cycle.

The compressive stress along the interface of the workpieces at the end of ten hold cycles followed the same trend developed during the squeeze cycle, but the magnitude has almost doubled. Nugget thermal expansion and the associated thermal stresses are the main contributors in the increased stress along this interface. The maximum stress near the periphery is 60 ksi (413.7 kPa) and it drops down to a minimum of 42.5 ksi (293 kPa) at the center. It is believed that the high stress buildup at the workpiece faying surface is due to stress concentration around the nugget area. These stresses did not extend to the surrounding area and to the electrode.

The displacement of the electrode due to nugget expansion was predicted from calculations to cause a final electrode indentation into the workpiece of 2.38 X 10^{-4} in. Also seen was that the workpiece rotated about the contact area due to mechanical response to thermal expansion.

Parametric Studies

Based on simulation results, the finite element model was further utilized to conduct a parametric study in which the effects of changing welding current, unequal workpiece thicknesses and dissimilar material on weld nugget formation were studied. The finite element model used to study the effect of unequal workpiece thickness was modified to include both upper and lower workpieces and electrodes in two quadrants.

Effect of Changing Welding Current

In this theoretical study, the model and materials previously used (copper electrode Class III and Type 347 stainless steel sheet 0.04 in. thick) were used again. The percentage of weld nugget penetration relative to the sheet thickness was chosen as a parameter. Different welding currents ranging from below 6000 A to above 10,000 A were selected. For each welding current, weld cycles required to form a weld nugget having 25, 50 and 75% penetration were established and used. Three curves rep-

Fig. 11 — The relationship between weld time and weld current for three different nugget penetrations. (% sheet thickness)

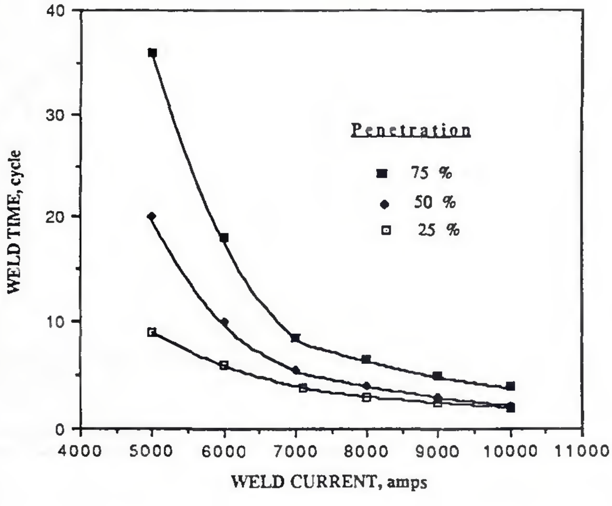

resenting each percentage were generated and plotted in Fig. 11. These curves show that for higher penetration, the required welding time increases rapidly as the weld current is reduced. These results are similar to the resistance welding lobe curves. The line to the far left represents the smallest nugget diameter acceptable and the line to the far right represents the largest nugget diameter acceptable before expulsion. For the theoretical studies, nugget penetration was used as a criterion rather than nugget diameter.

Effect of Unequal Thickness Workpieces

The modified finite element model used 347 stainless steel, 1000 lb loading and 8000 A welding current. The upper workpiece was 0.04 in. (1 mm) thick and the lower workpiece was 0.06 in. (1.5 mm) thick.

Figure 12 shows the model nugget area after seven weld cycles. The weld nugget was found more in the thicker workpiece than in the thinner workpiece. The reason for this unbalanced formation of the weld nugget is that the heat conduction path in the thinner workpiece was shorter than the path in the thicker workpiece. Therefore, the heat generated in the thicker piece had more time to raise the temperature of a larger area of the material before it was conducted away by the water-cooled electrode. This is in agreement with the results predicted by Refs. 1–4. The effect of the thermal conductivity of the material and the role of the electrode geometry are quite pronounced in this situation. Normal practice is that the electrode face diameter in contact with the thicker piece is larger than that of the other electrode to create a heat balance and proper nugget formation.

Effect of Dissimilar Material

In this study, equal thickness workpieces of 0.04 in. were chosen. For the upper workpiece AISI 1045 carbon steel was selected. Type 347 stainless steel was selected for the lower workpiece. Again, the load applied was 1000 lb, and the welding current used 8000 A. The total weld time was set to seven cycles.

Figure 13 shows the final weld nugget area, which was more in the stainless steel than in the carbon steel. The thermal properties of the materials significantly influence the mechanism of weld nugget formation and the final nugget geometry. Since the stainless steel has a higher electrical resistivity than the 1045 carbon steel, more heat was generated in the stainless steel workpiece than in the carbon steel workpiece. Also, be-

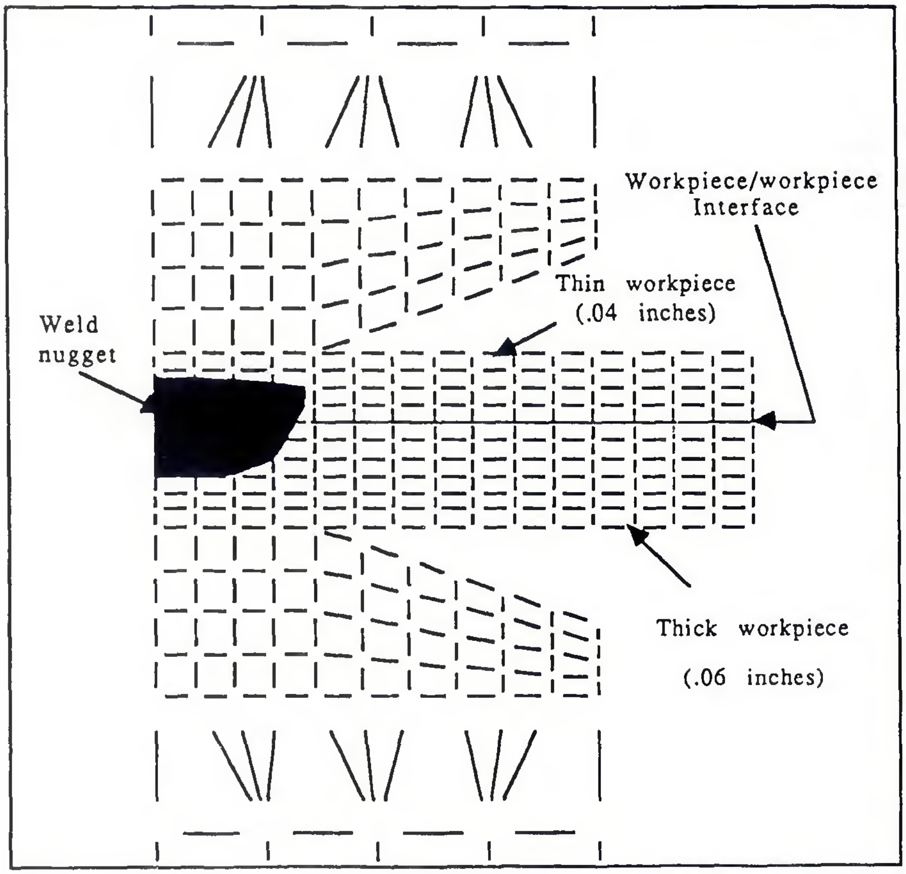

Fig. 12 — Weld nugget geometry obtained for unequal thickness workpieces after seven weld cycles. (8000 A)

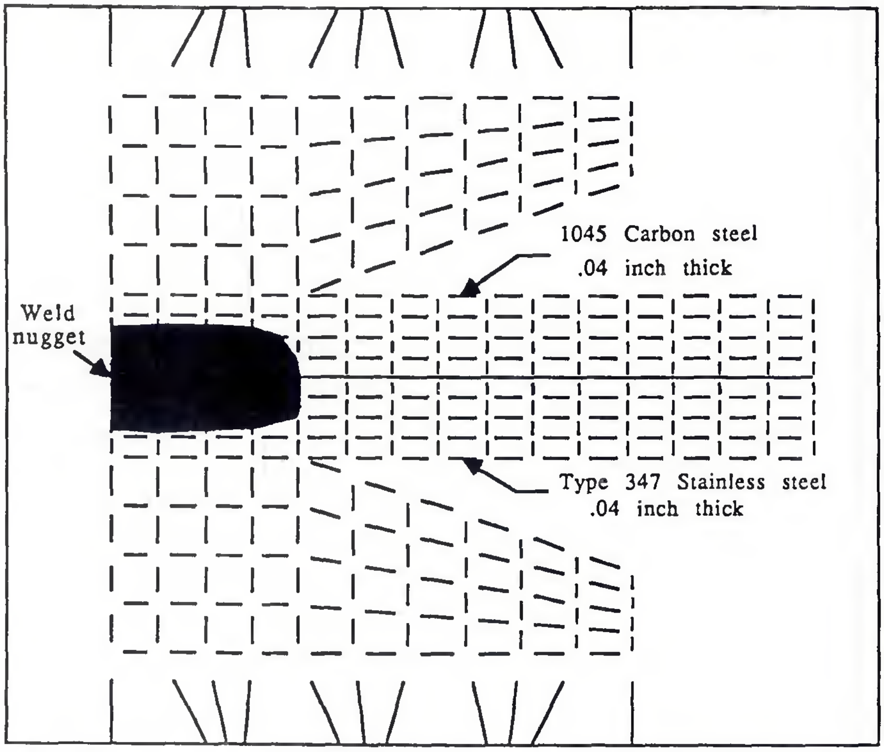

Fig. 13 — Weld nugget geometry obtained for equal thickness workpieces after seven weld cycles. (8000 A)

cause of the lower thermal conductivity of stainless steel, the heat was confined in a localized area and was conducted away slower. This slower thermal conduction enhanced nugget growth in the stainless steel workpiece more than in the carbon steel workpiece. This result was stated by similar arguments presented in Refs. 1–4.

Conclusions

The finite element model has provided detailed information regarding the state of stress attained during the squeeze cycle, which show stress concentration at the periphery of electrode/workpiece interface and the workpiece faying surface. The resultant diameter between the two workpieces was found to be larger than the electrode face diameter.

A ring-like weld nugget was initiated at a distance from the electrode center and expands inward and outward during the weld cycle. The weld nugget at the end of the hold cycle experiences different loads of stresses. These stresses are those generated by the electrodes during the squeeze cycle and developed during thermal expansion and contraction caused by the weld and hold cycles, respectively. The final nugget geometry was obtained at the end of hold cycle. A comparison of the numerical predictions with the experimental data showed good qualitative agreement.

However, several other factors or phenomena associated with resistance spot welding were not studied in this paper. Contact resistance at the interfaces, coefficient of friction at the interfaces, stress distribution at the end of the hold cycle, weld expulsion mechanism, welding of galvanized or other types of coated steels and electrode dimension and end geometry are important parameters that need to be investigated.

References

1. *Resistance Welding Manual*. Third Edition, Vols. 1 and 2, Resistance Welder Manufacturers' Association, 1972.
2. Cary, H. 1979. *Modern Welding Technology*. Prentice-Hall, Inc.
3. *Welding Handbook*. Seventh Edition, Vol. 3, American Welding Society, Miami, Fla.
4. Roberts, W. L. 1951. Resistance variations during spot welding. *Welding Journal* 30(11):1004–1019.
5. Houchens, A. F., Page, R. E., and Yang, W. H. 1977. Numerical modeling of resistance spot welding. *Proceedings of Numerical Modeling Manufacturing Processes*, ASME Winter Conference, pp. 117–129.
6. Gould, J. E. 1987. An examination of nugget development during resistance spot welding using both experimental and analytical techniques. *Welding Journal* 66(1): 1-s to 10-s.
7. Nied, H. A. 1984. The finite modeling of the resistance spot welding process. *Welding Journal* 63(4) 123-s to 132-s.
8. Dickinson, D. W., Franklin, J. E., and Stanya, A. 1980. Characterization of spot welding behavior of dynamic electrical parameter monitoring. *Welding Journal* 59(6): 170-s to 176-s.
9 Kaiser, J. G., Dunn, G. J., and Eagar, T. W. 1982. The effect of electrical resistance on nugget formation during spot welding. *Welding Journal* 61(6):167-s to 174-s.
10. Savage, W. F., Nippes, E. F., and Wassell, F. A. 1987. Dynamic contact resistance of series spot welds. *Welding Journal* 57(2):43-s to 50-s.
11. Bowden, F. P., and Williamson, J. B. P. 1958. Electrical conduction in solid-I: influence of the passage of current on the contact between solids. *Proc. Roy. Soc. London*, pp. 1–12.
12. Greenwood, J. A., and Williamson, J. B. P. 1958. Electrical conduction in solid-II: theory of temperature-dependent conductors. *Proc. Roy. Soc. London*, pp. 13–31.
13. Archer, G. R. 1960. Calculations for temperature response in spot welds. *Welding Journal* 39(8):327-s to 330-s.
14. Greenwood, J. A. 1961. Temperature in spot welding. *Brit. Weld. Journal* (6): 316–322.
15. Bentley, K. P., Greenwood, J. A., Knowlson, P., and Baker, R. G. 1963. Temperature distributions in spot welds. *Brit. Weld. Journal*, pp. 613–619.
16. Rice, W., and Funk, E. J. 1967. An analytical investigation of the temperature distributions during resistance welding. *Welding Journal* 46(4):175-s to 186-s.
17. Civelek, M. S., Erdogan, F., and Cakiroglu, A. O. 1978. Interface separation for an elastic layer loaded by a rigid stamp. *Int. J. Engr. Sci.*, pp. 669–679.